Article ID: 1000-324X(2022)11-1245-14 **DOI:** 10.15541/jim20220114

Nd-doped Mesoporous Borosilicate Bioactive Glass-ceramic Bone Cement

CHEN Cheng[1], DING Jingxin[1], WANG Hui[2], WANG Deping[1]

(1. School of Materials Science and Engineering, Tongji University, Shanghai 201804, China; 2. Engineering Research Center of Traditional Chinese Medicine Intelligent Rehabilitation, Ministry of Education, Institute of Rehabilitation Medicine, School of Rehabilitation Science, Shanghai University of Traditional Chinese Medicine, Shanghai 201203, China)

Abstract: As a common malignant bone tumor, osteosarcoma is usually treated by surgical resection. However, the bone defects caused by surgery are difficult to heal, and the possibility of osteosarcoma recurrence can also be increased by the residual tumor cells. Therefore, a Nd-doped mesoporous borosilicate bioactive glass-ceramic bone cement was developed for repair of bone defects and synergistic therapy of osteosarcoma. Firstly, as photothermal agent and drug carrier, Nd-doped mesoporous borosilicate bioactive glass-ceramic (MBGC-*x*Nd) microspheres were prepared through Sol-Gel method and solid-state reaction. Then MBGC-*x*Nd microspheres were mixed with sodium alginate (SA) solution to prepare injectable bone cement (MBGC-*x*Nd/SA). The results showed that Nd^{3+} endows microspheres with controllable photothermal properties, and microspheres loaded with doxorubicin (DOX) showed sustained drug release behavior. In addition, the drug release from drug-loaded bone cement was significantly accelerated with the increase of temperature, indicating that the heat generated by photothermal therapy had the possibility of promoting the release of DOX. *In vitro* cell experiment results showed that MBGC-*x*Nd/SA had good osteogenic activity. Simultaneously, photothermal-chemical combination therapy had a more significant killing effect on MG-63 osteosarcoma cells, indicating a synergistic effect. Therefore, MBGC-*x*Nd/SA, as a novel multifunctional bone repair material, exhibits a potential application in the postoperative treatment of osteosarcoma.

Key words: Nd-doped mesoporous borsilicate bioactive glass-ceramic; bone cement; bone defect repair; photo-thermal-chemical combination therapy

As a malignant bone tumor, osteosarcoma is often found in adolescents, posing a serious threat to their health[1]. Most osteosarcoma can be treated by surgical resection, but it is difficult to prevent the recurrence and metastasis of residual tumor cells[2]. At the same time, the resection of osteosarcoma leads to serious bone defects, which seriously damage the health of patients[3]. Therefore, it is significant for the comprehensive treatment of osteosarcoma to develop biomaterials with both anti-tumor function and bone tissue repair function.

In recent years, due to the excellent biological activity and degradation properties, bioactive glass bone cement has been widely studied in bone defect repair[4]. Bioactive glass bone cement is prepared by mixing bioactive glass powder and the liquid phase, and then injected into the bone defect site by a minimally invasive method. It provides mechanical support for the early self-healing period after solidification. Meanwhile, the functional ions released from bioactive glass can effectively promote the regeneration of bone tissue[5-6]. In our previous research, borosilicate bioactive glass with controllable degradation properties was prepared by replacing part of SiO_2 of silicate bioactive glass by B_2O_3, and the divalent cations released by the degradation of borosilicate bioactive glass were chelated with liquid alginate, which enhanced the handling performance and biological activity of bone cement[7-9]. In addition, we have reported that mesoporous borosilicate bioactive glass microspheres were loaded with drug molecules and used as smart carriers for local drug slow-release[10].

Received date: 2022-03-02; **Revised date:** 2022-04-03; **Published online:** 2022-05-07
Foundation item: National Natural Science Foundation of China (52172286, 51772210); National Key R&D Program of China (2018YFC1106302)
Biography: CHEN Cheng (1997–), male, Master candidate. E-mail: 1930642@tongji.edu.cn
陈 铖(1997–), 男, 硕士研究生. E-mail: 1930642@tongji.edu.cn
Corresponding author: WANG Hui, associate professor. E-mail: WHIL86@shutcm.edu.cn;
WANG Deping, professor. E-mail: wdpshk@tongji. edu.cn
王 会, 副研究员. E-mail: WHIL86@shutcm.edu.cn;
王德平, 教授. E-mail: wdpshk@tongji.edu.cn

In addition to repairing bone defects, killing residual tumor cells is also an indispensable task in the postoperative treatment of osteosarcoma. Photothermal therapy (PTT) and chemotherapy (CHT) are common adjuvant treatments after tumor surgery, and the combination of the two has been proven to have certain advantages in improving tumor treatment efficiency and reducing side effects[11-13]. This is because the heat generated by PTT can both kill tumor cells and accelerate the entry of drug molecules into tumor cells[11]. In addition, tumor cells are more sensitive to chemical drugs when heated, which helps to improve the treatment efficiency of anti-cancer drugs[14]. Yang *et al*.[15] synthesized a redox-responsive drug delivery system, which effectively inhibited the growth of lung cancer cells through photothermal-chemotherapy function. Zhao *et al*.[16] developed a hollow polymer-silica nanohybrid as a nanocarrier to simultaneously deliver the photothermal agent and anti-cancer drug to tumors for chemo-photothermal synergistic therapy, which achieved better therapeutic effects in the treatment of high-grade malignant tumor models. However, there are currently few reports on the research of PTT&CHT combination therapy for osteosarcoma. So it deserves to try to use the combination therapy to improve the treatment effect of osteosarcoma.

Among rare earth ions, Nd^{3+} with excellent photothermal properties, can be effectively excited by the 808 nm laser located in the first biological window and has a larger absorption cross section[17-18]. With increasing doping concentration, Nd^{3+} has a concentration quenching effect, which makes heavily neodymium-doped nanoparticles contain a highly light-to-heat conversion efficiency[19]. At the same time, Nd^{3+} doped biomaterials show good biocompatibility[20-21].

Accordingly, in this study, we first prepared neodymium-doped mesoporous borosilicate bioactive glass-ceramic (MBGC-*x*Nd) microspheres with good photothermal properties through the Sol-Gel method combined with solid-state reaction[22], and used it for loading an anticancer drug doxorubicin (DOX). Subsequently, as solid phase, MBGC-*x*Nd microspheres were mixed with sodium alginate (SA) solution to obtain a multifunctional bone cement (MBGC-*x*Nd/SA) for regeneration of bone tissue and synergistic therapy of osteosarcoma (Scheme 1). The microscopic morphology, phase composition and mesoporous structure of MBGC-*x*Nd microspheres were characterized. The photothermal properties and DOX release behavior of microspheres and bone cement were characterized, and setting properties of bone cement were tested. The biological activity of promoting proliferation and differentiation of rabbit bone mesenchymal stem cells (rBMSCs) of the prepared bone cement were preliminarily evaluated *in vitro*. In addition, the killing effect of PTT&CHT combination therapy on osteosarcoma cells (MG-63) was also evaluated.

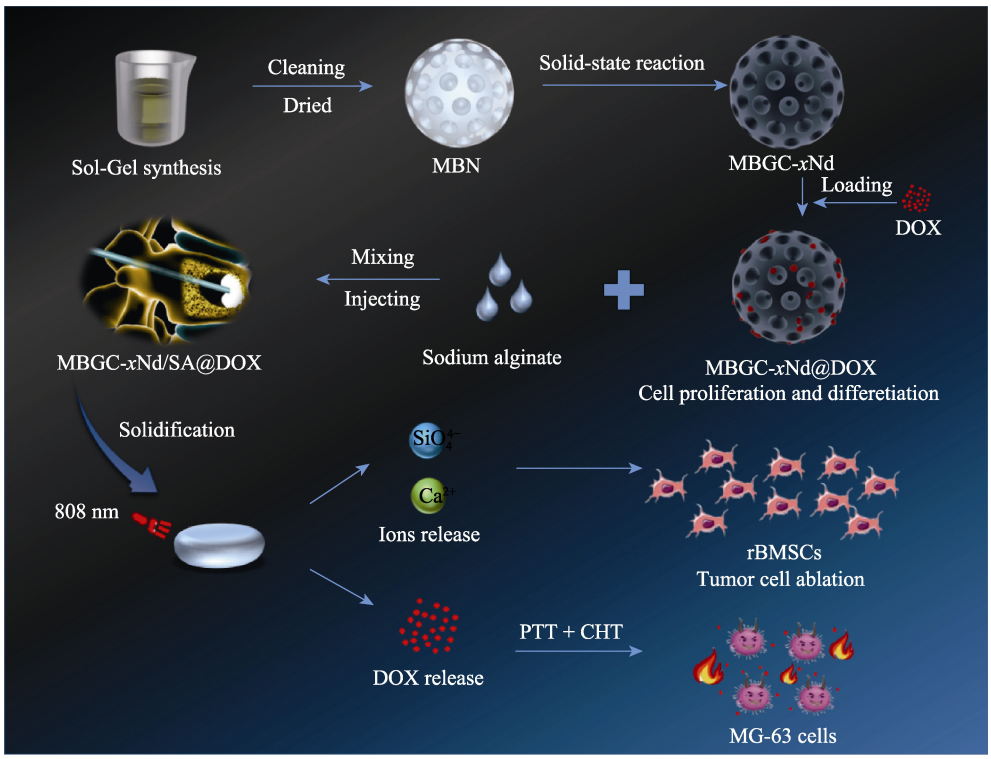

Scheme 1 Schematic diagram of preparation and properties of MBGC-*x*Nd microspheres and MBGC-*x*Nd/SA bone cement
The color figure can be obtained from online edition

1 Materials and Methods

1.1 Materials

Tri-n-butyl borate (TBB), neodymium nitrate hexahydrate ($Nd(NO_3)_3·6H_2O$), calcium nitrate tetrahydrate ($Ca(NO_3)_2·4H_2O$), tetraethyl orthosilicate (TEOS), ammonia solution (25 % NH_3 in water, in mass), ethyl acetate, ethanol absolute, triethylphosphate (TEP), doxorubicin hydrochloride, cetyl trimethyl ammonium bromide (CTAB), sodium alginate (SA), gluconolactone, and Na_2HPO_4 were purchased from Sinopharm Chemical Reagent Co., Ltd (Shanghai, China). The BCA protein concentration determination kit, fetal bovine serum (FBS), dexamethasone, alkaline phosphate assay kit, beta-glycerophosphate disodium salt, and Vitamin C were purchased from Beyotime Biotechnology (Shanghai, China). Low-glucose dulbecco's modified eagle medium (DMEM), high-glucose DMEM, 1% penicillin/streptomycin, and CCK-8 reagent were purchased from Titan Scientific Co., Ltd (Shanghai, China). MG-63 cells and rBMSCs were obtained from Shanghai Sixth People's Hospital.

1.2 Preparation of MBGC-*x*Nd microspheres

The mesoporous SiO_2-B_2O_3-P_2O_5 nanospheres (MBN) were prepared through the Sol-Gel method[23], and their chemical composition (in mol) was 78% SiO_2+16% B_2O_3+6% P_2O_5. Firstly, 0.7 g CTAB and 20 mL ethyl acetate were added into 40 mL deionized water under stired at 30 ℃. 30 min later, 0.7 mL ammonia solution were added. Later, 2.43 mL TEOS, 1.67 mL TBB and 0.288 mL TEP were added every 30 min. After 4 h, the reaction solution was centrifuged to collect the precipitate. After washed three times by absolute ethanol and deionized water, the precipitate was vacuum dried at 37 ℃ to obtain MBN.

MBGC-*x*Nd microspheres were prepared *via* solid-state reaction[22]. The composition of MBGC-*x*Nd microspheres is shown in Table 1, where Nd^{3+} replaced Ca^{2+} in an equimolar ratio (x=0, 0.01, 0.03, 0.05). The specific process was as follows. A certain amount of calcium nitrate tetrahydrate and neodymium nitrate hexahydrate was dissolved in 40 mL absolute ethanol. Then MBN was added, and the suspension was stirred until absolute ethanol was completely volatilized. The collected powder was annealed at 600 ℃ for 5 h to prepare MBGC-*x*Nd microspheres.

Table 1 Composition in molar percent of MBGC-*x*Nd microspheres

Sample	SiO_2	B_2O_3	P_2O_5	CaO	$NdO_{3/2}$
MBGC-0Nd	50	10	4	36	0
MBGC-1Nd	50	10	4	35	1
MBGC-3Nd	50	10	4	33	3
MBGC-5Nd	50	10	4	31	5

1.3 Preparation of MBGC-*x*Nd/SA

2 g SA, 1 g gluconolactone and 3 g Na_2HPO_4 were dissolved in 100 mL deionized water to form a solution, which, as the liquid phase, was mixed and stirred with MBGC-*x*Nd microspheres at a liquid-solid ratio of 1.3 mL/mg. After stirred for 60 s, the bone cement slurry was poured into a ϕ6 mm×12 mm polytetrafluoroethylene cylindrical mold for molding, then stored at 37 ℃ for 24 h.

1.4 Characterization of MBN, MBGC-*x*Nd microspheres and MBGC-3Nd/SA

The microscopic morphology of MBN and MBGC-*x*Nd microspheres was observed by transmission electron microscope (TEM; H-800; Japan). The phase composition of MBN and MBGC-*x*Nd microspheres was tested by X-ray polycrystalline diffractometer (XRD; Rigaku SmartLab 9; Japan). The mesoporous parameters of MBN and MBGC-*x*Nd microspheres were tested by specific surface area analyzer (BET; Autosorb-Nova 2200 e; America). After dried and sprayed with gold, the morphology of MBGC-3Nd/SA was observed *via* scanning electron microscope (SEM; S-4700; Japan).

1.5 Characterization of degradation performance

The degradation performance of MBGC-*x*Nd microspheres was characterized by measuring the change of Ca and Si concentrations in simulated body fluid (SBF). MBGC-*x*Nd microspheres were soaked in SBF at pH 7.4 (1 mg/mL), then stored at 37 ℃. After 1, 3, 7, and 10 d, Ca and Si concentrations were tested through inductively coupled plasma emission spectrometer (ICP; PE 8300; America).

1.6 Drug loading and release

1.6.1 Drug loading of MBGC-*x*Nd microspheres

Firstly, 0.25 mg/mL DOX-PBS solution was configured by dissolving doxorubicin hydrochloride in phosphate buffer solution (PBS). Then 50 mg MBGC-*x*Nd microspheres were added in 6 mL DOX solution. After shaking for 1 d, the solution was centrifuged, the supematant was collected, and precipitated MBGC-*x*Nd@DOX microspheres were obtained and dried at 37 ℃. Next, DOX standard solutions (0.006–0.06 mg/mL) were configured, and their DOX concentration was tested by ultraviolet-visible spectroscope (UV-Vis; U-4100; Japan) at an absorption wavelength of 480 nm[23]. The obtained standard curve equation between the measured standard concentration of DOX and the absorbance value was as follows.

$$A = 18.78954 \cdot C + 0.0326 \quad (1)$$

(R^2=0.9992), where A is the absorbance value, C is the DOX concentration.

Absorbance value of the above-mentioned centrifuged supernatant was measured, then substituted into the Eq.(1) to obtain the concentration of residual DOX in the solution. Finally, the DOX encapsulation efficiency (E) was calculated by Eq. (2)[23]:

$$E = (C_i - C_r) / C_i \cdot 100\% \quad (2)$$

Where C_t is the initial DOX concentration, and C_r is the residual DOX concentration.

1.6.2 Drug release from MBGC-*x*Nd@DOX microspheres

The dried MBGC-*x*Nd@DOX microspheres were soaked in 7 mL PBS at pH 4.7, and shaken at 120 r/min in a 37 ℃ shaker. After shaking for 1, 3, 6, 9, 12, 24, 48, 72, 168, and 240 h, 3.5 mL solution was aspirated to measure the DOX concentration and new PBS was supplemented. The cumulative concentration of DOX released from MBGC-*x*Nd@DOX microspheres was calculated by Eq. (3)[24]:

$$C_{t,\mathrm{cum}} = C_t + 0.5 \cdot \sum_{0}^{t-1} C_t \quad (3)$$

Where C_t is the DOX concentration of the solution at time t (t = 1, 3, 6, 9, 12, 24, 48, 72, 168, and 240 h). Five parallel experiments were tested and the average DOX cumulative concentration was calculated.

1.6.3 Drug release from MBGC-*x*Nd/SA drug-loaded bone cement

MBGC-*x*Nd/SA drug-loaded bone cement (MBGC-*x*Nd/SA@DOX) was obtained by mixing MBGC-*x*Nd@DOX microspheres and sodium alginate solution. The prepared MBGC-*x*Nd/SA@DOX (6 mm×6 mm×3 mm) were immersed in 7 mL PBS at pH 4.7 for the drug release experiment. For characterizing the influence of temperature on the DOX release behavior, the temperature of the shaker was adjusted to 35, 45 and 55 ℃ to carry out the drug release experiment of MBGC-3Nd/SA@DOX.

1.7 Characterization of photothermal properties

For studying the influence of Nd^{3+} doping amount on photothermal properties of MBGC-*x*Nd microspheres, 3.2 W/cm^2 808 nm laser was used to irradiate MBGC-*x*Nd microspheres with different Nd^{3+} doping amounts for 5 min with an on and off cycle for five times. The MBGC-0Nd microsphere was used as a control sample. An infrared thermal camera system (Fluke, Everett, WA, America) was used to record temperature changes in time. In addition, different power densities of 808 nm lasers (0.56, 0.99, 1.5, and 3.2 W/cm^2) were used for irradiating MBGC-3Nd microspheres to characterize the influence of power densities of laser on the photothermal properties of microspheres.

Furthermore, bone cement samples were soaked in 10 mL SBF and irradiated under 2.4 W/cm^2 laser to characterize the photothermal properties of MBGC-0Nd/SA and MBGC-3Nd/SA after five switching cycles.

1.8 Setting properties of MBGC-*x*Nd/SA

1.8.1 Setting time measurement

The setting time was recorded according to ISO 9917-1. The bone cement slurry was prepared by above method and poured into a ϕ6 mm×12 mm polytetrafluoroethylene cylindrical mold. The bone cement slurry was considered to be set when the needle (1.13 mm in diameter, 400 g in weight) of the Vicat instrument fell freely on the surface of the bone cement and failed to cause obvious indentation (indentation depth≤0.5 mm). The setting time was defined as a period from the preparation of the slurry to the set of the slurry. The average setting time was calculated by testing five parallel experiments.

1.8.2 Injectability measurement

Bone cement slurry was squeezed out from a syringe (1.7 mm in diameter) at a loading rate of 15 mm/min until the indenter pressure reached 100 N. Injectability (Inj.) was calculated as follows:

$$\mathrm{Inj.} = (W_2 - W_0) / (W_1 - W_0) \cdot 100\% \quad (4)$$

Where W_0 is the weight of the empty syringe, W_1 is the weight of the syringe containing bone cement slurry, and W_2 is the weight of the syringe containing the residual bone cement slurry. The average injectability was calculated by testing five parallel experiments.

1.8.3 Compressive strength measurement

The bone cement samples cured for 24 h in a box with constant temperature and humidity were taken out, and the surface moisture was wiped with filter paper. After the upper and lower surfaces of the samples were polished with sandpaper into parallel surfaces, the samples were placed in an electronic universal testing machine (CTM250; China), and loaded at 0.5 mm/min loading rate to measure compressive strength. The average compressive strength was calculated by testing five parallel experiments.

1.8.4 Anti-washout properties measurement

After curing for 24 h and drying, bone cement samples were soaked in PBS at pH 7.4 (0.2 g/mL), then placed in a 37 ℃ gas bath thermostat and oscillated at the rate of 180 r/min. After oscillating for 6, 12, 18 and 24 h, the samples were taken out and dried. The anti-washout properties were calculated by Eq. (5):

$$\mathrm{R.} = W_t / W_0 \cdot 100\% \quad (5)$$

Where R. is the remaining weight ratio, W_0 is the initial dry weight of the bone cement, W_t is the remaining dry weight of the bone cement at time t (t=6, 12, 18, and

24 h). The average value was calculated by testing five parallel experiments.

1.9 Cell viability test of rBMSCs

1.9.1 Test of cell proliferation

BMSCs were cultured in low-glucose DMEM containing 10% FBS and 1% penicillin/streptomycin in cell incubator (ESCO, Singapore) in condition of 37 ℃ and 5% CO_2. The bone cement samples were prepared to a size of ϕ6 mm×3 mm for *in vitro* cell experiments. The samples were autoclaved and immersed in low-glucose DMEM (100 mg/mL). After 24 h, the extract of the bone cement samples was collected through filter membrane and diluted 40 times with low-glucose DMEM. The rBMSCs were seeded in 96-well plates (500 cells/well) and cultured in low-glucose DMEM for 1 d. Next, the diluted DMEM containing extract was added to replace the previous medium and replaced every two days. After culturing for 1, 3 and 5 d, the OD value was tested by CCK-8 reagent. The average OD value was calculated by testing five parallel experiments.

1.9.2 Test of alkaline phosphatase (ALP) activity

The osteogenic differentiation ability was evaluated by measuring ALP activity of rBMSCs cultured in the bone cement extract[25]. The bone cement extract was diluted 40 times with low-glucose DMEM, then added with a final concentration of 10 mmol/L β-glycerophosphate disodium salt, 0.1 μmol/L dexamethasone, and 50 μmol/L Vitamin C to configure the osteogenic differentiation medium. The rBMSCs were seeded in 48-well plates (2×10^4 cells/well) and cultured in low-glucose DMEM for 1 d. Then the osteogenic differentiation medium was added to replace the previous medium and replaced every 2 d. The ALP activity was evaluated on the 7th and 14th days by alkaline phosphate assay kit. After staining for 30 min, the optical density (OD) value was tested at 405 nm. At the same time, the cell protein content in each well was tested through the BCA protein concentration determination kit. The OD value divided by the total cell protein content to calculate the relative ALP activity. The average value was calculated by testing five parallel experiments.

1.10 Anti-tumor experiment of PTT&CHT combination therapy

MG-63 osteosarcoma cells were cultured in high-glucose DMEM containing 10% FBS and 1% penicillin/streptomycin in cell incubator in condition of 37 ℃ and 5% CO_2. Then MG-63 cells were seeded in 48-well plates (2×10^4 cells/well). After 1 d of incubation, the autoclaved MBGC-0Nd/SA, MBGC-3Nd/SA, and MBGC-3Nd/SA@DOX were placed in 48-well plates, and each group of bone cement samples was divided into the laser irradiation group and the non-laser irradiation group. MBGC-0Nd/SA without laser irradiation was used as a blank control group. MBGC-3Nd/SA with laser irradiation, MBGC-3Nd/SA@DOX without laser irradiation and MBGC-3Nd/SA@DOX with laser irradiation were labeled as PTT group, CHT group and CHT&PTT combination therapy group. Then the laser irradiation group was irradiated under 2.4 W/cm^2 808 nm laser for 5 min. After co-culturing for 12 h, the previous medium and bone cement were removed, and 50 μL CCK-8 reagent and 450 μL high-glucose DMEM were added. Two hours later, the OD value was tested. Finally, the OD value of the blank control group was regarded as 100%, and the proportion of the OD value of the other groups accounting for the OD value of the blank control group was calculated to obtain the tumor cell survival rate. The average value was calculated by testing five parallel experiments.

1.11 Statistical analysis

The experimental results were represented as mean± standard deviation, and statistical analysis was performed *via* one-way ANOVA. When $p<0.05$ (*), the data were considered significantly different.

2 Results and discussion

2.1 Characterization of MBGC-*x*Nd microspheres

As shown in Fig. 1(a-e), all microspheres were in regular spherical shape with diameters about 250 nm, and displayed obvious slit-type mesoporous structure, which was attributed to the removal of the templating agent CTAB. Compared with MBN, the internal structure of MBGC-*x*Nd microspheres was more compact. It showed that the morphology and size of MBN were not significantly affected by the introduction of Ca^{2+} and Nd^{3+} through solid-state reaction, but the mesoporous structure of microspheres was affected to some extent (Fig. 1(f)).

Fig. 1(g) showed the phase composition of MBN and MBGC-*x*Nd microspheres after heat treatment at 600 ℃. It obviously exhibits broad peaks existed in all samples, which were attributed to the glass phase structure of MBN, while the solid-state reaction of introducing Ca^{2+} and Nd^{3+} produced a clear crystalline phase composition. All MBGC-*x*Nd microsphere data showed diffraction peaks at 2θ=32.4° and 33.2°, which were in line with the diffraction characteristic peaks of $Ca_2SiO_4\cdot0.05Ca_3(PO_4)_2$ (PDF#49-1674). However, the data of MBGC-3Nd and MBGC-5Nd microspheres showed diffraction peaks at 2θ=25.8° and 31.8°, which were in line with the diffraction characteristic peaks of $Ca_8Nd_2(PO_4)_6O_2$ (PDF#32-0175). Especially, the diffraction characteristic peaks of Nd_2O_3 (PDF#65-3184) appeared in MBGC-5Nd microsphere

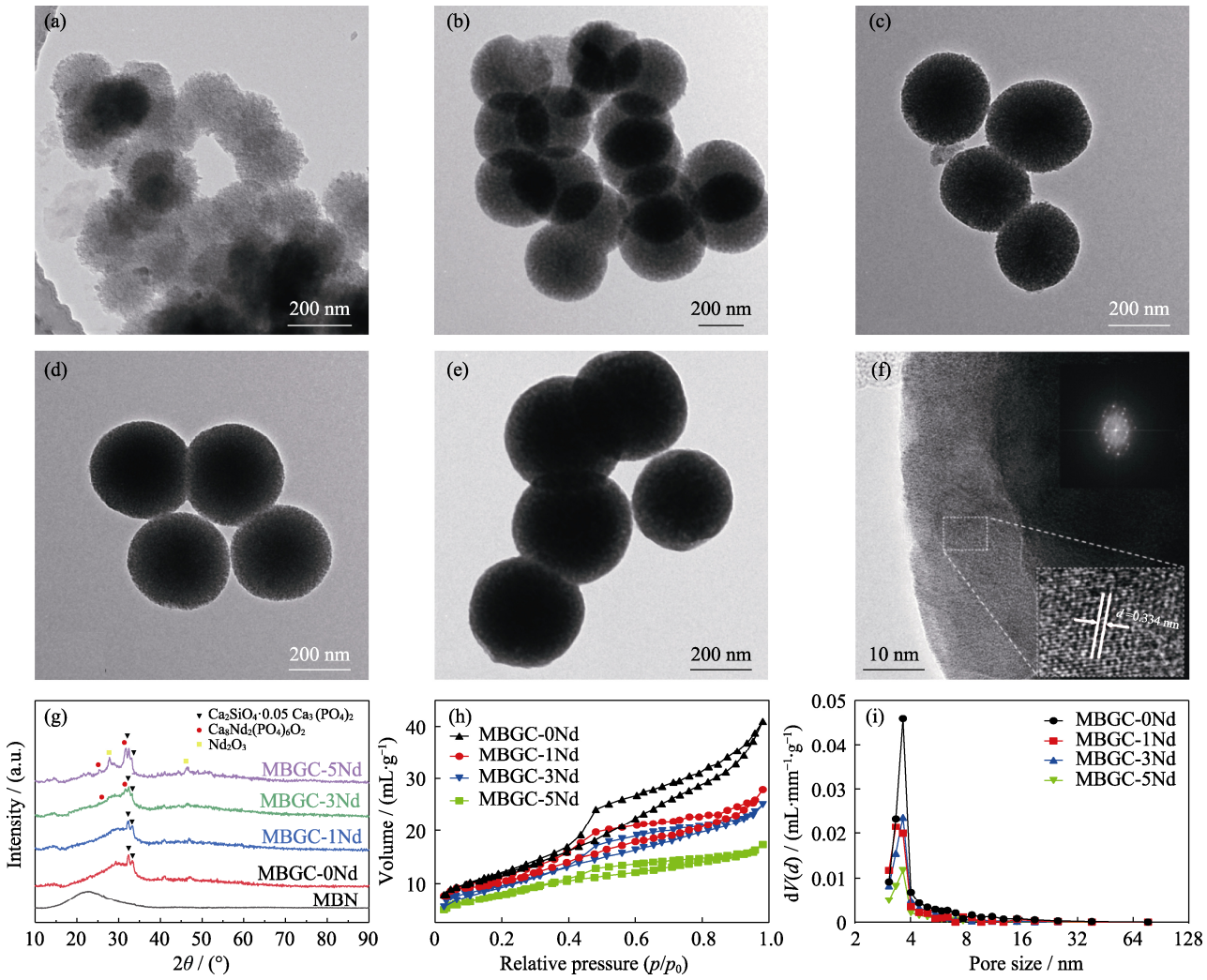

Fig. 1 Characterization of MBGC-*x*Nd microspheres

(a-e) TEM images of (a) MBN, (b) MBGC-0Nd microspheres, (c) MBGC-1Nd microspheres, (d) MBGC-3Nd microspheres, and (e) MBGC-5Nd microspheres; (f) High-resolution TEM image of MBGC-3Nd microspheres with insert showing the interplanar crystal spacing at about 0.334 nm; (g) XRD patterns of MBN and MBGC-*x*Nd microspheres; (h) N_2 adsorption-desorption isotherm and (i) pore size distribution curve of MBGC-*x*Nd microsphere

The color figures can be obtained from online edition

data at 2θ=27.9° and 46.3°. In order to prevent Nd^{3+} with high ionic potential from destroying the balance of the microemulsion system, the solid-state reaction was used to incorporate Ca^{2+} and Nd^{3+} into MBN. Therefore, it can be considered that Ca^{2+} and Nd^{3+} were deposited on the surface and pores of MBN by adsorption. Ca^{2+} and Nd^{3+} gradually diffused into the glass network and competed for non-bridging oxygen during the sintering process, causing an increase in free energy of the system, promoting the formation of crystalline phases[26]. In addition, the results also showed that the final crystalline phase composition might be affected by the relative content of Ca^{2+} and Nd^{3+}.

As can be seen from Fig. 1(f), the amorphous morphology existed in the MBGC-3Nd microspheres, and the diffraction fringes of the crystals were also distributed in the microspheres. The interplanar crystal spacing was around 0.334 nm, which was consistent with the lattice spacing of (002) plane of $Ca_8Nd_2(PO_4)_6O_2$. The results showed that the crystal phase generated during the solid-state reaction existed in the glass phase in the form of dispersed crystallites. Type IV isotherm and H3 hysteresis loop were seen in all N_2 adsorption-desorption isotherms of MBGC-*x*Nd microspheres, revealing the slit-type mesoporous structure of microspheres (Fig. 1(h)). However, with the increase of Nd^{3+} content, the hysteresis loop of MBGC-*x*Nd microspheres got smaller, demonstrating the reduction of specific surface area. The pore size distribution range of MBGC-*x*Nd microspheres was narrow, mainly in the range of 3–8 nm (Fig. 1(i)).

As shown in Table 2, compared with MBN, the specific surface area, pore size, and pore volume of MBGC-*x*Nd microspheres reduced. This is because Ca^{2+} and Nd^{3+} were deposited on the surface and pores of MBN by

Table 2　Pore structure of MBN and MBGC-*x*Nd microspheres

Sample	Specific surface area/($m^2 \cdot g^{-1}$)	Pore size /nm	Pore volume /($cm^3 \cdot g^{-1}$)
MBN	329.261	12.506	0.4498
MBGC-0Nd	42.092	6.024	0.0634
MBGC-1Nd	36.065	4.776	0.0431
MBGC-3Nd	34.424	4.496	0.0387
MBGC-5Nd	28.818	3.710	0.0268

adsorption, and gradually diffused into the glass network during the sintering process. Therefore, there might be some formed microcrystalline phase stacking in the pores, resulting in a decrease in these mesoporous parameters[22]. In addition, the pore size of MBGC-*x*Nd microspheres decreased with the increase of Nd^{3+} content. When Nd^{3+} doping concentration was low, it replaced Ca^{2+} as network modifier[27-28]. The ionic radii of Nd^{3+} and Ca^{2+} were similar, but the charge of Nd^{3+} was higher. Therefore, Nd^{3+} with higher ionic potential might enable the glass network tighter, resulting in the shrinkage of the mesoporous structure.

Bioactive glass in the body fluid environment can release functional ions (such as Ca^{2+} and SiO_4^{4-}), which play a significant role in promoting bone regeneration[4,7]. MBGC-*x*Nd microspheres showed obvious degradation in SBF by releasing Ca and Si (Fig. 2). At the early stage, the Si and Ca concentrations increased rapidly, then Si concentration remained relatively stable and Ca concentration even decreased. It is because a large amount of free SiO_4^{4-} and Ca^{2+} on the surface of the microspheres were released into the solution at the initial stage. As the Si concentration reached saturation, SiO_4^{4-} began to accumulate on the surface to form a silicon-rich layer[7]. Ca^{2+} reacted with PO_4^{3-} in the solution to form hydroxyapatite deposited on the surface, consuming the Ca^{2+} in the solution[29]. Besides, the ionic degradation rate of MBGC-*x*Nd decreased with the rise of Nd^{3+} content, which was attributed to the progressively strengthened glass network. On the one hand, with the reduction of specific surface area, the contact area between microspheres and SBF decreased, and on the other hand, it was difficult in releasing ions.

Adequate drug loading content and sustained drug release behavior are essential for effective chemotherapy. The results showed the encapsulation efficiency of MBGC-0Nd, MBGC-1Nd, MBGC-3Nd, and MBGC-5Nd microspheres was 89.2%, 84.6%, 82.3%, and 73.8%, respectively. As can be observed in Fig. 3(A), all MBGC-*x*Nd@DOX microspheres showed the sustained drug release behavior. As the Nd^{3+} content increasing, the total amount of DOX released during the whole period decreased from about 45% (MBGC-0Nd) to about 35% (MBGC-5Nd). It is due to the influence of Nd^{3+} content on the mesoporous structure of microspheres, and the decrease of these mesoporous parameters resulted in the reduction of DOX encapsulation efficiency and the difficulty in drug release. In addition, for such mesoporous microspheres, DOX is mainly loaded by mesoporous through physical adsorption[10]. However, the degradation of microspheres is caused by ion exchange between the glass network and surrounding solution. Therefore, DOX based on physical adsorption exerted less effect on the degradation process based on chemical action. However, the accumulative amount of DOX released from MBGC-3Nd during the whole period could increase with the temperature rising and attain more than 55% Fig. 3(B), which obviously indicated that temperature might be used as an effective way to control the release.

The photothermal properties of MBGC-*x*Nd microspheres were characterized under 808 nm near-infrared laser irradiation. The microspheres doped with Nd^{3+} showed a rapid rise of temperature under 3.2 W/cm^2 808 nm laser irradiation, and maintained a stable heating effect during the five switching cycles of the laser (Fig. 4(A-C)),

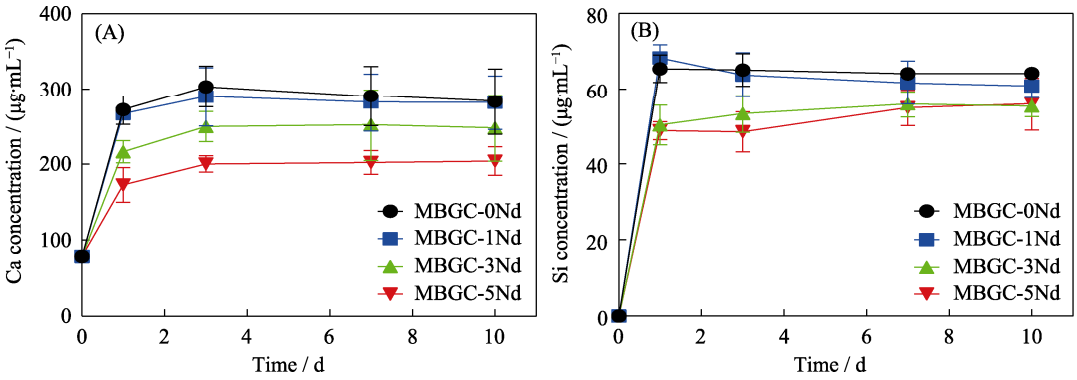

Fig. 2　Changes of (A) Ca and (B) Si concentrations with MBGC-*x*Nd microspheres in SBF

The color figures can be obtained from online edition

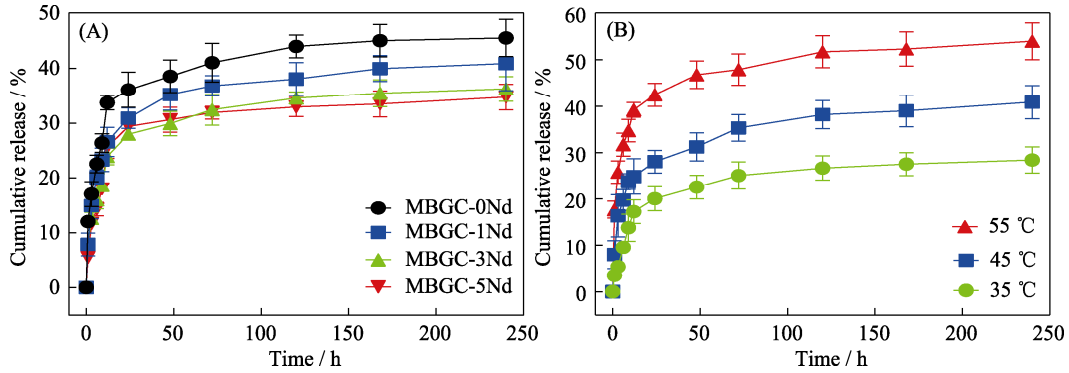

Fig. 3 Cumulative release curves of DOX from (A) MBGC-*x*Nd@DOX microspheres in PBS at pH 4.7 and (B) MBGC-3Nd/SA@DOX in PBS at pH 4.7 under different ambient temperatures

The color figures can be obtained from online edition

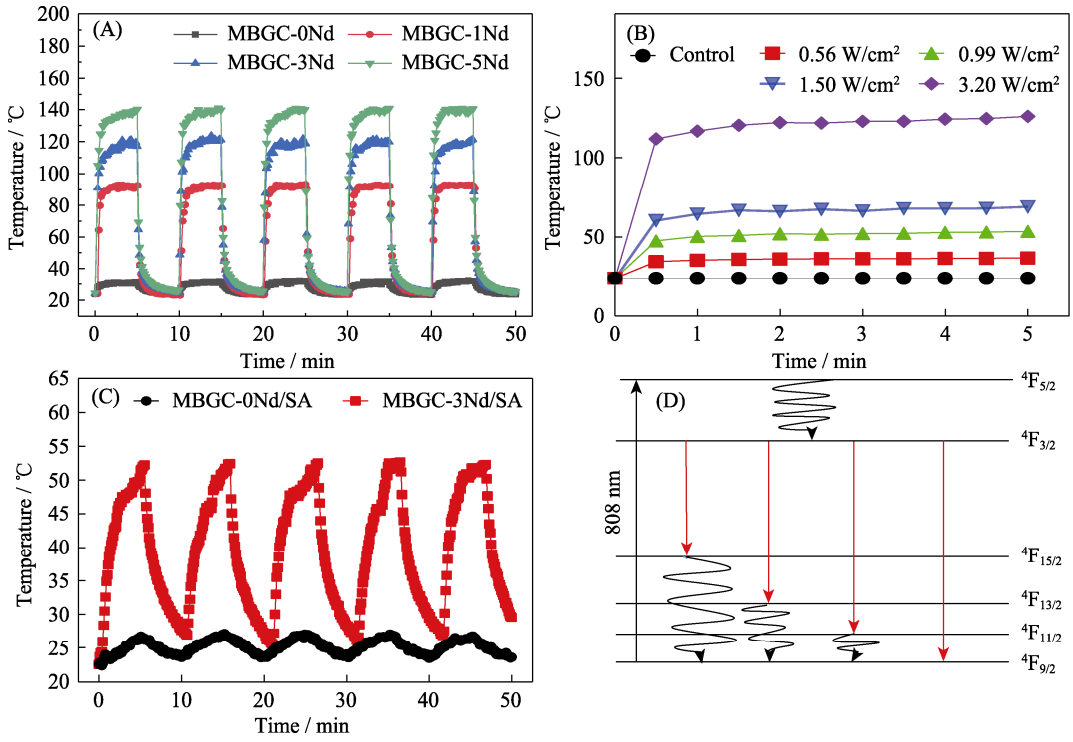

Fig. 4 Photothermal properties of MBGC-*x*Nd microspheres

(A) Heating curves of MBGC-*x*Nd microspheres under 808 nm laser irradiation (3.2 W/cm^2); (B) Heating curves of MBGC-3Nd microspheres under 808 nm laser irradiation at different power densities; (C) Heating curves of MBGC-3Nd/SA immersed in SBF under 808 nm laser irradiation (2.4 W/cm^2); (D) Energy level diagram of Nd^{3+}

The color figures can be obtained from online edition

while MBGC-0Nd microspheres did not show the photothermal effect (Fig. 4(A)). Meanwhile, the final temperature of MBGC-*x*Nd microspheres rose with the increase of Nd^{3+} content. Nd^{3+} ([Xe]4f^3) has particular electronic configuration with a half-filled 4f orbit. As Fig.4(D) showed, electrons are excited to an excited state ($4F_{5/2}$) under the laser irradiation of 808-nm, then rapidly return to the metastable ground state $4F_{3/2}$ by the nonradiative process. Later, Nd^{3+} undergoes a radiative decay to lower energy states (such as $4F_{13/2}$, $4F_{11/2}$ and $4F_{9/2}$), and the phonon-assisted decay occurs in the ground state, which results in photothermal effect[30-32]. In view of lower Nd^{3+} content and better photothermal properties, MBGC-3Nd microspheres were chosen for further experiments (Fig. 4(C)). With the increase of power density, a growing tendency was represented in the final temperature of MBGC-3Nd microspheres under the irradiation of 808 nm laser (Fig. 4(B)).

2.2 Characterization of MBGC-3Nd/SA bone cement

The prepared MBGC-3Nd/SA bone cement showed excellent injectability (Fig. 5(A)). The MBGC-3Nd microspheres were coated with sodium alginate to prepared MBGC-3Nd/SA and formed a whole through cross-linking.

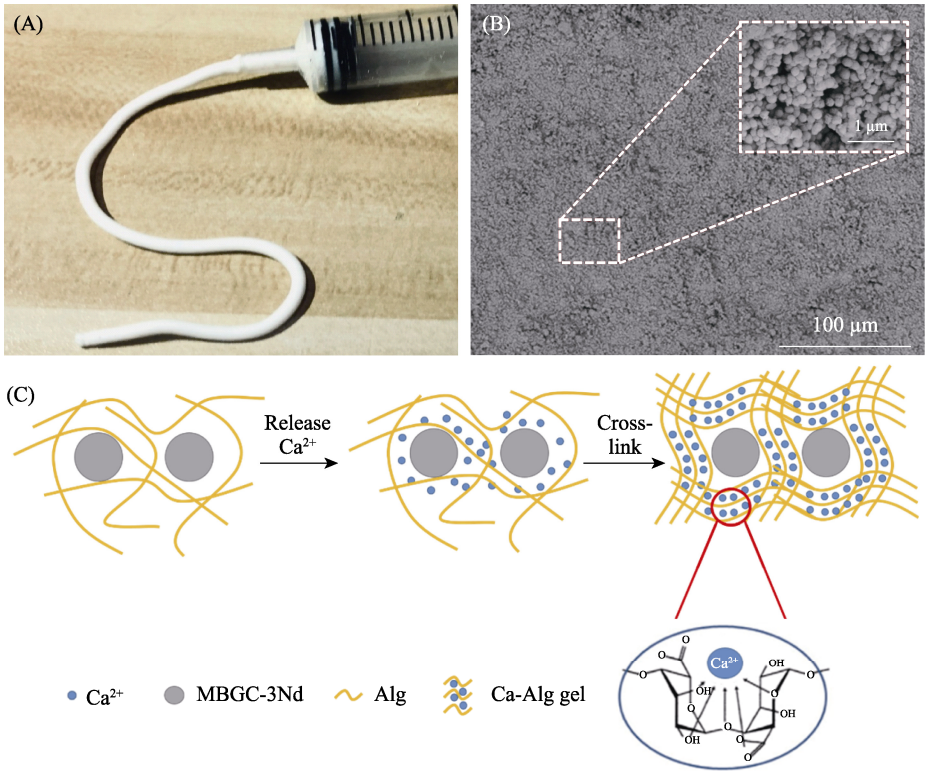

Fig. 5　Characterization of MBGC-3Nd/SA bone cement

(A) Photo of extruded bone cement; (B) SEM image of MBGC-3Nd/SA; (C) Schematic illustration of the setting process of MBGC-3Nd/SA

The color figures can be obtained from online edition

However, the bone cement was not completely dense, and there were some gaps between the clusters formed by the cross-linking of the microspheres and alginate, which might facilitate the drug release from the bone cement (Fig. 5(B)). As shown in Fig. 5(C), when MBGC-3Nd microspheres were in contact with the liquid phase, the surface glass network was destroyed, and Ca^{2+} were released from the surface, which then cross-linked with alginate on the glass surface to form the Ca-Alg gel[7-9]. With the continuous dissolution of Ca^{2+}, the generated Ca-Alg gel gradually wrapped the microspheres like a packaging bag to form a whole, and gradually realized the coagulation and solidification of the bone cement. Moreover, previous studies have shown that borates can be complexed with diols in the sugar ring of alginate, leading to formation of mono- and di-complexes[33-34]. This indicated that the B component might play a prominent role in the cross-linking process of MBGC-3Nd microspheres and alginate.

The influence of Nd^{3+} content on the setting properties of MBGC-*x*Nd/SA is shown in Fig. 6. With the increase of Nd^{3+} content, the setting time of bone cement increased from about 27 min to about 34 min (Fig. 6(A)). The reason lied in the crosslinking speed between MBGC microspheres and alginate depends on the dissolution speed of Ca^{2+}, which gradually decreases with the increase of Nd^{3+} content, resulting in prolonged setting time of bone cement. In addition, the cumulative dissolution concentration of Ca^{2+} of microspheres also decreased with the increase of Nd^{3+} content, resulting in insufficient cross-linking with alginate and a decrease in the compressive strength of bone cement (Fig. 6(C)). As shown in Fig. 6(B), more than 90% of the bone cement slurry was extruded from the syringe within 2 min, and there was no significant difference in the injection rate of all bone cement samples, indicating that the incorporation of Nd^{3+} exerted no significant effect on the injectability of bone cement. It can be seen from Fig. 6(D) that with the rise of Nd^{3+} content, the remaining mass of samples reduced, indicating the anti-washout property gradually weakened. However, the remaining mass of all samples was more than 90%, demonstrating the good anti-washout property. In summary, MBGC-*x*Nd/SA performed good operability and suitable for clinical minimally invasive surgery.

As shown in Fig. 4(C), the temperature of MBGC-3Nd/SA immersed in SBF increased rapidly under 2.4 W/cm^2 808 nm laser irradiation and reached about 53 ℃, then maintained a stable heating effect within five switching cycles of the laser. According to previous

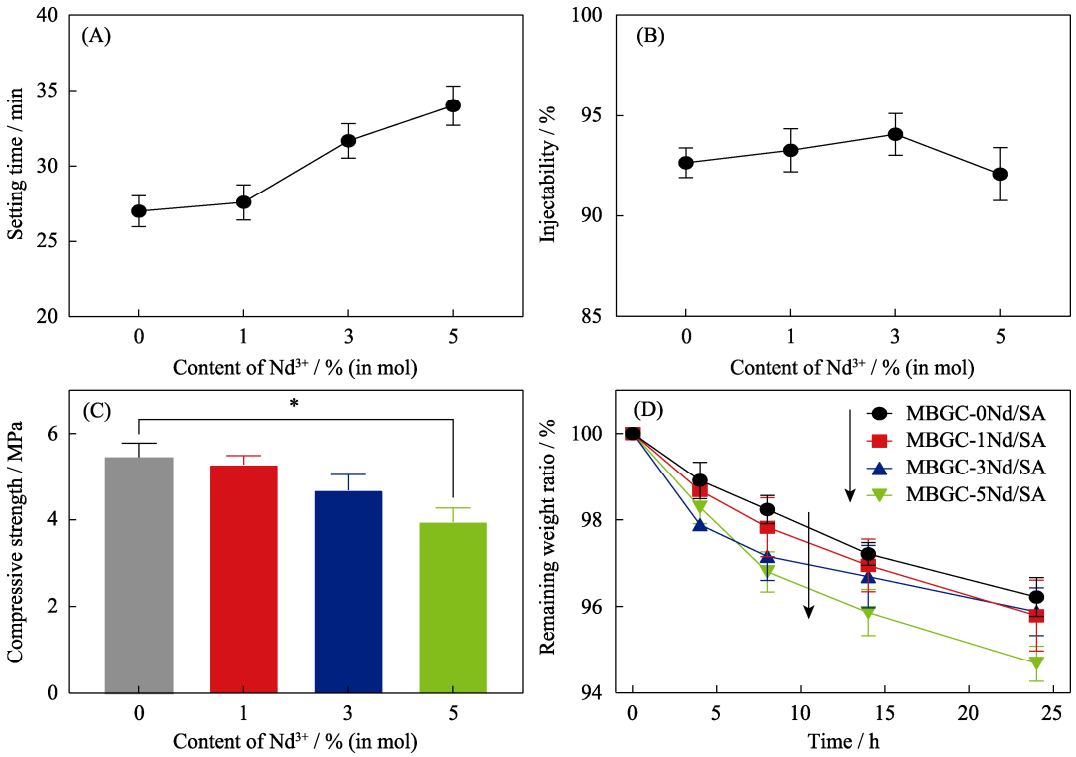

Fig. 6 Setting properties of MBGC-*x*Nd/SA

(A) Setting time; (B) Injectability; (C) Compressive strength; (D) Anti-washout property. *: $p<0.05$ ($n=5$)

The color figures can be obtained from online edition

studies, the suitable temperature for photothermal therapy is about 53 ℃, which not only effectively inhibits tumor growth, but also causes less damage to tissues[20,35]. Meanwhile, MBGC-0Nd/SA did not exhibit obvious photothermal properties under the same laser irradiation. The results show that the photothermal properties of MBGC-3Nd were not affected by the alginate composition. In addition, at different ambient temperatures, the sustained drug release behavior of MBGC-3Nd/SA@DOX was exhibited, and the cumulative release of DOX increased with the rise of ambient temperature, which may be the result of faster diffusion of DOX at higher temperature (Fig. 3(B)). This result demonstrates the heat generated by the photothermal therapy possessed the possibility of promoting the release of DOX. According to the previous studies, the IC_{50} data of DOX on MG-63 osteosarcoma cells was 3.87 μg/mL[36], while in the high DOX concentration of 50 μg/mL, the survival rate of rat mesenchymal stem cells after 48 h culturing was still higher than 50%[37]. This indicates that the cytotoxicity of DOX to osteosarcoma cells is much higher than to mesenchymal stem cells. Therefore, it is possible to avoid photothermal-promoted release of DOX to destroy the osteogenic function by adjusting the drug loading and the laser irradiation time.

Fig. 7 showed the effects of MBGC-0Nd/SA and MBGC-3Nd/SA extracts on the osteogenic properties of rBMSCs. As can be seen from Fig. 7(A), compared with the blank control, rBMSCs cultured in MBGC-0Nd/SA and MBGC-3Nd/SA bone cement extracts showed higher viability on the fifth day, reflecting their effect of promoting cell proliferation. Meanwhile, no significant difference was seen in the proliferation behavior of rBMSCs between MBGC-0Nd/SA and MBGC-3Nd/SA extracts, indicating that the cytocompatibility of bone cement was not affected by the incorporation of Nd^{3+}. Furthermore, the alkaline phosphate (ALP) activity of rBMSCs was shown to be stimulated by extracts of MBGC-0Nd/SA and MBGC-3Nd/SA (Fig. 7(B)). These results suggest that the MBGC-*x*Nd/SA bone cement possesses good cytocompatibility and bioactivity to promote the proliferation and expression of ALP activity of rBMSCs. Previous studies have also shown that borosilicate bioactive glass bone cement has good biocompatibility and can promote new bone regeneration in rabbit femoral condyle defects[38]. It is thus reasonable to believe that the MGBC-*x*Nd bone cement might be used as a bioactive material to repair bone defects.

Previous studies have shown that benefiting from the release of active ions such as SiO_4^{4-} and Ca^{2+}, which can promote the formation of hydroxyapatite, borosilicate bioactive glass has good bioactivity and can promote bone tissue regeneration[39-42]. In addition, borate with low concentrations can stimulate cell growth and proliferation

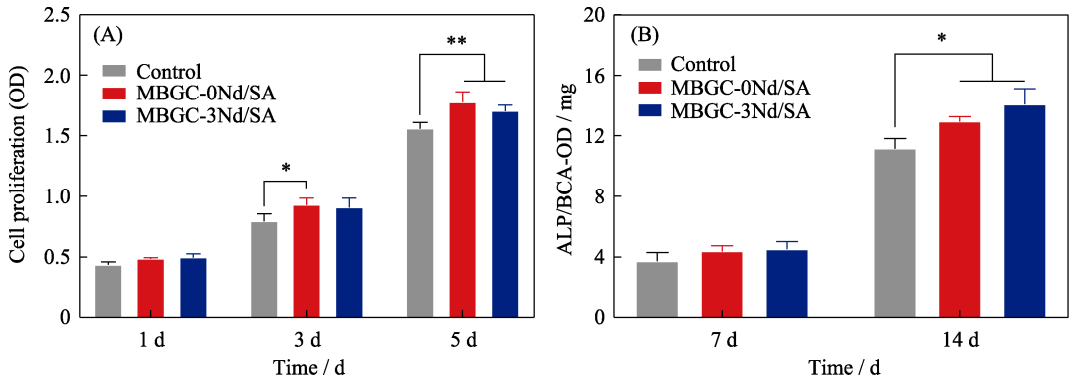

Fig. 7　(A) Proliferation results and (B) alkaline phosphate activity of rBMSCs cultured in the bone cement extract
*: $p < 0.05$; **: $p < 0.01$. ($n = 5$).
The color figure can be obtained from online edition

by activating the MAPK pathway[43]. Recently, Ma *et al*.[20] reported that Nd-doped bioglass has high bioactivity in stimulating angiogenesis, which improves the ability to promote tissue regeneration. It is thus reasonable to believe that MBGC-*x*Nd/SA might be a bioactive material which could promote the regeneration of bone tissue. However, the mechanisms of Nd^{3+} in regulating cellular activity need to be investigated by further studies.

As shown in Fig. 8(A), the relative survival of co-cultured MG-63 cells decreased from (95.82±3.81)% to (25.15±2.35)% after MBGC-3Nd/SA was irradiated by 2.4 W/cm^2 808 nm laser for 5 min, while no significant difference was seen in the relative survival of MG-63 cells co-cultured with MBGC-0Nd/SA before and after the laser irradiation. This result indicated that the photothermal therapy of MBGC-3Nd/SA had obvious killing effect on MG-63 cells. Furthermore, compared with PTT or CHT, the relative survival of MG-63 cells under combination therapy was significantly lower, only (7.04±3.32)%, indicating the synergistic effect of PTT&CHT combination therapy (Fig. 8(B)). Indeed, MG-63 cells are human osteosarcoma cells, and it possesses the property of both osteoblast like cells and tumor like cells. Furthermore, it also can differentiate into osteoblasts under the induction of growth factor. Due to the poorer heat dissipation capacity, tumor tissue has been shown to be more thermosensitive than normal tissue[44-45]. Therefore, during the anti-tumor treatment state, PTT can selectively kill the tumor cells with harmless effects on the normal cells. In addition, according to our previous studies, localized pH rises with the degradation of borosilicate bioactive glass[7]. Such a slightly alkaline environment can promote the proliferation of osteoblasts[46] but inhibit the proliferation of tumor cells.

In recent years, due to the efficacy and selectivity, PTT has received much attention in bone tumor therapy. Ma *et al*.[47] fabricated a graphene oxide-*β*-tricalcium phosphate composite stent by 3D printing and surface modification strategy, which combined significantly improved osteogenic capacity with a high photothermal effect. Chen *et al*.[48] developed a novel functional tricalcium silicate bone cement with excellent photothermal properties for minimally invasive treatment of bone tumors. Liu *et al*.[49] prepared Mn-doped mesoporous bioactive glass as a phototherapy agent for bone regeneration and bone tumor treatment. However, PTT has a major shortcoming: the heat applied to the tumor is often uneven, leading to some cancer cells escape to survive and recurrence[16,50]. Therefore, it is significant to combine PTT with other therapy methods to improve the therapy efficiency of bone tumor. As we all know, CHT is a traditional therapy method for cancer treatment that can significantly inhibit the tumor growth rate. Previous studies have shown that the combination of PTT and CHT achieved a significant synergistic effect[51-53]. In this study, the developed MBGC-3Nd/SA bone cement not only maintained the good bioactivity of borosilicate bioactive glass-ceramics, but also performed simultaneous photothermal therapy and chemotherapy on osteosarcoma cells by using MBGC-3Nd microspheres as photothermal agents and anti-cancer drug carriers. The combination therapy of PTT and CHT showed a significant synergistic effect on osteosarcoma cells, which improved the therapy efficiency. Hence, the combination of PTT and CHT is a potential therapy strategy with high efficacy for the synergistic therapy of osteosarcoma.

3　Conclusion

In this work, a Nd-doped mesoporous borosilicate bioactive glass-ceramic bone cement (MBGC-*x*Nd/SA) for repair of bone defects and synergistic therapy of osteosarcoma is prepared by mixing Nd-doped mesoporous borosilicate bioactive glass-ceramic (MBGC-*x*Nd) microspheres and sodium alginate (SA) solution. The results

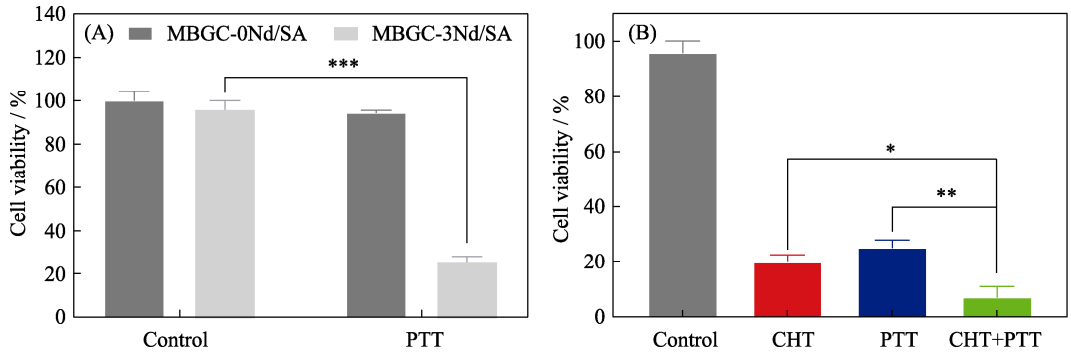

Fig. 8 Relative survival of MG-63 cells co-cultured with (A) bone cement under 808 nm laser irradiation at a power density of 2.4 W/cm^2 for 5 min and (B) MBGC-3Nd/SA under PTT, CHT or combination therapy. *: p<0.05; **: p<0.01, ***: p<0.001 (n=5)
The color figures can be obtained from online edition

demonstrate that Nd^{3+} endowed MBGC-*x*Nd microspheres with controllable photothermal properties, which can be adjusted by changing Nd^{3+} content and the power density of NIR laser. MBGC-*x*Nd microspheres loaded with DOX all show sustained drug release behavior, but the mesoporous structure of MBGC-*x*Nd microspheres shrinks with the incorporation of Nd^{3+} content, resulting in a slower degradation rate and a lower DOX encapsulation efficiency. The prepared MBGC-3Nd/SA bone cement exhibits good photothermal properties, and the heat generated by the photothermal therapy has the possibility of promoting the release of DOX. In addition, MBGC-3Nd/SA exhibits osteogenic bioactivity of promoting the proliferation and the expression of alkaline phosphatase activity of rBMSCs *in vitro*. More importantly, the synergistic effect of photothermal-chemical combination therapy of MBGC-3Nd/SA is demonstrated in tumor cell experiments. All above results consolidate that MBGC-3Nd/SA can be a promising material for postoperative treatment of osteosarcoma.

References:

[1] RAINUSSO N, WANG L L, YUSTEIN J T. The adolescent and young adult with cancer: state of the art-bone tumors. *Current Oncolology Reports*, 2013, **15(4):** 296–307.

[2] BALLATORI S E, HINDS P W. Osteosarcoma: prognosis plateau warrants retinoblastoma pathway targeted therapy. *Signal Transduction Target Therapy*, 2016, **1:** 16001–12.

[3] LIAO J F, SHI K, JIA Y P, *et al*. Gold nanorods and nanohydroxyapatite hybrid hydrogel for preventing bone tumor recurrence *via* postoperative photothermal therapy and bone regeneration promotion. *Bioactive Materials*, 2021, **6(8):** 2221–2230.

[4] WANG W H, YEUNG K W K. Bone grafts and biomaterials substitutes for bone defect repair: a review. *Bioactive Materials*, 2017, **2(4):** 224–247.

[5] CUI X, ZHANG Y D, WANG H, *et al*. An injectable borate bioactive glass cement for bone repair: preparation, bioactivity and setting mechanism. *Journal of Non-Crystalline Solids*, 2016, **432:** 150–157.

[6] CUI X, ZHAO C J, GU Y F, *et al*. A novel injectable borate bioactive glass cement for local delivery of vancomycin to cure osteomyelitis and regenerate bone. *Journal of Material Science: Mater ials in Medicine*, 2014, **25(3):** 733–745.

[7] XIE X, PANG L B, YAO A H, *et al*. Nanocement produced from borosilicate bioactive glass nanoparticles composited with alginate. *Australian Journals of Chemistry*, 2019, **72(5):** 354–361.

[8] CHANG Y C , ZHAO R L , WANG H, *et al*. A novel injectable whitlockite-containing borosilicate bioactive glass cement for bone repair. *Journal of Non-Crystalline Solids*, 2020, **547:** 120291–11.

[9] WU Z F, LIN Z Y, YAO A H, *et al*. Influence of particle size distribution on the rheological properties and mathematical model fitting of injectable borosilicate bioactive glass bone cement. *Ceramics International*, 2020, **46(15):** 24395– 24406.

[10] PANG L B, WANG D P. Drug carrier based on mesoporous borosilicate glass microspheres. *Journal of Inorganic Materials*, 2022, **37(7):** 780-786.

[11] LI J, ZHANG C T, GONG S M, *et al*. A nanoscale photothermal agent based on a metal-organic coordination polymer as a drug-loading framework for effective combination therapy. *Acta Biomaterialia*, 2019, **94:** 435–446.

[12] ZHAO Q F, WANG X D, YANG M, *et al*. Multi-stimuli responsive mesoporous carbon nano-platform gated by human serum albumin for cancer thermo-chemotherapy. *Colloids Surface B Biointerfaces*, 2019, **184:** 110532–11.

[13] ZHANG T, JIANG Z Q, XVE T, *et al*. One-pot synthesis of hollow PDA@DOX nanoparticles for ultrasound imaging and chemo-thermal therapy in breast cancer. *Nanoscale*, 2019, **11(45):** 21759–21766.

[14] WANG L L, HERVAULT A, SOUTHERN P, *et al*. *In vitro* exploration of the synergistic effect of alternating magnetic field mediated thermo-chemotherapy with doxorubicin loaded dual pH- and thermo-responsive magnetic nanocomposite carriers. *Journal of Materials Chemistry B*, 2020, **8(46):** 10527–10539.

[15] YANG Y, LIN Y Z, DI D H, *et al*. Gold nanoparticle-gated mesoporous silica as redox-triggered drug delivery for chemo-photothermal synergistic therapy. *Journal of Colloid Interface Science*, 2017, **508:** 323–331.

[16] ZHAO L Z, YUAN W, THAM H P, *et al*. Fast-clearable nanocarriers conducting chemo/photothermal combination therapy to inhibit recurrence of malignant tumors. *Small*, 2017, **13(29):** 1700963–9.

[17] ROSAL B D, ROCHA U, XIMENDES E C, *et al*. Nd^{3+} ions in nanomedicine: perspectives and applications. *Optical Materials*, 2017, **63:** 185–196.

[18] ROSAL B D, DELGADO A P, CARRASCO E, *et al*. Neodymium-based stoichiometric ultrasmall nanoparticles for multifunctional deep-tissue photothermal therapy. *Advanced Optical Materials*, 2016, **4(5):** 782–789.

[19] ROCHA U, CARLOS J, SILVA W F, *et al*. Sub-tissue thermal sensing based on neodymium-doped LaF_3 nanoparticles. *ACS Nano*, 2013, **7(2):** 1188–1199.

[20] MA L L , ZHOU Y L, ZHANG Z W B, *et al*. Multifunctional bioactive Nd-Ca-Si glasses for fluorescence thermometry, photothermal therapy, and burn tissue repair. *Science Advances*, 2020, **6(32):** eabb1311–12.

[21] ROCHA U, KUMAR K U, JACINTO C, *et al*. Neodymium-doped LaF_3 nanoparticles for fluorescence bioimaging in the second biological window. *Small*, 2014, **10(6):** 1141–1154.

[22] XIE W H, CHEN X Y, LI Y L, *et al*. Facile synthesis and *in vitro* bioactivity of radial mesoporous bioactive glass with high phosphorus and calcium content. *Advanced Powder Technology*, 2020, **31(8):** 3307–3317.

[23] WANG X, WANG G, ZHANG Y. Research on the biological activity and doxorubicin release behavior *in vitro* of mesoporous bioactive SiO_2-CaO-P_2O_5 glass nanospheres. *Applied Surface Science*, 2017, **419:** 531–539.

[24] ZHU Y F, KOCKRICK E, IKOMA T, *et al*. An efficient route to rattle-type Fe_3O_4@SiO_2 hollow mesoporous spheres using colloidal carbon spheres templates. *Chemistry of Materials*, 2009, **21:** 2547–2553

[25] TIAN T, HAN Y, MA B, *et al*. Novel Co-akermanite ($Ca_2CoSi_2O_7$) bioceramics with the activity to stimulate osteogenesis and angiogenesis. *Journal of Materials Chemistry B*, 2015, **3(33):** 6773–6782.

[26] WARREN B E, PINCUS A G. Atomic consideration of immiscibility in glass systems. *Journal of American Ceramics Society*, 1940, **23:** 301–304.

[27] ANAND V, SINGH K J, KAUR K. Evaluation of zinc and magnesium doped 45S5 mesoporous bioactive glass system for the growth of hydroxyl apatite layer. *Journal of Non-Crystalline Solids*, 2014, **406:** 88–94.

[28] SANCHEZ-SALCEDO S, MALAVASI G, SALINAS A J, *et al*. Highly-bioreactive silica-based mesoporous bioactive glasses enriched with gallium(III). *Materials (Basel)*, 2018, **11(3):** 367–17.

[29] ZHOU J, WANG H, ZHAO S C, *et al*. *In vivo* and *in vitro* studies of borate based glass micro-fibers for dermal repairing. *Material Science Engineering C: Materials for Biological Application*, 2016, **60:** 437–445.

[30] STOUWDAM J W, VEGGEL F. Near-infrared emission of redispersible Er^{3+}, Nd^{3+}, and Ho^{3+} doped LaF_3 nanoparticles. *Nano Letters*, 2002, **2(7):** 733–737.

[31] WANG X F, LIU Q, BU Y Y, *et al*. Optical temperature sensing of rare-earth ion doped phosphors. *RSC Advances*, 2015, **5(105):** 86219–86236.

[32] HEMMER E, ACOSTA-MORA P, MENDEZ-RAMOS J, *et al*. Optical nanoprobes for biomedical applications: shining a light on upconverting and near-infrared emitting nanoparticles for imaging, thermal sensing, and photodynamic therapy. *Journal of Materials Chemistry B*, 2017, **5(23):** 4365–4392.

[33] BALAKRISHNAN B, JAYAKRISHNAN A. Self-cross-linking biopolymers as injectable *in situ* forming biodegradable scaffolds. *Biomaterials*, 2005, **26(18):** 3941–3951.

[34] BALAKRISHNAN B, JOSHI N, JAYAKRISHNAN A, *et al*. Self-crosslinked oxidized alginate/gelatin hydrogel as injectable, adhesive biomimetic scaffolds for cartilage regeneration. *Acta Biomaterialia*, 2014, **10(8):** 3650–3663.

[35] QU Y, ZHUANG H, ZHANG M, *et al*. Bone cements for therapy and regeneration for minimally invasive treatment of neoplastic bone defects. *Journal of Materials Chemistry B*, 2021, **9:** 4355–4364.

[36] LIN S W, LI X Q, LIU S Y, *et al*. Inhibition of combination of icaritin and doxorubicin on human osteosarcoma MG-63 cells *in vitro*. *Chinese Journal of Integrated Traditional & Western Medicine*, 2016, **36(6):** 729–734.

[37] ZHAO Y K, TANG S S, GUO J M, *et al*. Targeted delivery of doxorubicin by nano-loaded mesenchymal stem cells for lung melanoma metastases therapy. *Scientific Reports*, 2017, **7:** 44758.

[38] CUI X, ZHANG Y D, WANG J Y, *et al*. Strontium modulates osteogenic activity of bone cement composed of bioactive borosilicate glass particles by activating Wnt/*β*-catenin signaling pathway. *Bioactive Materials*, 2020, **5(2):** 334–347.

[39] PANG L B, SHEN Y F, HU H R, *et al*. Chemically and physically cross-linked polyvinyl alcohol-borosilicate gel hybrid scaffolds for bone regeneration. *Material Science Engineering C: Materials in Biological Application*, 2019, **105:** 110076–12.

[40] BI L X, RAHAMAN M N, DAY D E, *et al*. Effect of bioactive borate glass microstructure on bone regeneration, angiogenesis, and hydroxyapatite conversion in a rat calvarial defect model. *Acta Biomaterialia*, 2013, **9(8):** 8015–8026.

[41] GU Y F, HUANG W H, RAHAMAN M N, *et al*. Bone regeneration in rat calvarial defects implanted with fibrous scaffolds composed of a mixture of silicate and borate bioactive glasses. *Acta Biomaterialia*, 2013, **9(11):** 9126–9136.

[42] RAHAMAN M N, DAY D E, BAL B S, *et al*. Bioactive glass in tissue engineering. *Acta Biomaterialia*, 2011, **7(6):** 2355–2373.

[43] PARK M, LI Q, SHCHEYNIKOV N, *et al*. NaBCl is a ubiquitous electrogenic Na^+-coupled borate transporter essential for cellular boron homeostasis and cell growth and proliferation. *Mollecular Cell*, 2004, **16(3):** 331–341.

[44] NIKFARJAM M, MURALIDHARAN V, CHRISTOPHI C. Mechanisms of focal heat destruction of liver tumors. *Journal of Surgical Research*, 2005, **127:** 208–223.

[45] CHU K F, DUPUY D E. Thermal ablation of tumours: biological mechanisms and advances in therapy. *Nature Reviews Cancer*, 2014, **14(3):** 199–208.

[46] MONFOULRT L E, BECQUART P, MARCHAT D, *et al*. The pH in the microenvironment of human mesenchymal stem cells is a critical factor for optimal osteogenesis in tissue-engineered constructs. *Tissue Engineering Part A*, 2014, **20(13):** 1827–1840.

[47] MA H S, JIANG C, ZHAI D, *et al*. A bifunctional biomaterial with photothermal effect for tumor therapy and bone regeneration. *Advanced Functional Materials*, 2016, **26(8):** 1197–1208.

[48] XU C, MA B, PENG J L, *et al*. Tricalcium silicate/graphene oxide bone cement with photothermal properties for tumor ablation. *Journal of Materials Chemistry B*, 2019, **7(17):** 2808–2818.

[49] LIU Y Q, LIN R C, MA L L, *et al*. Mesoporous bioactive glass for synergistic therapy of tumor and regeneration of bone tissue. *Applied Materials Today*, 2020, **19:** 100578–14.

[50] ZHU X J, FENG W, CHANG J, *et al*. Temperature-feedback

upconversion nanocomposite for accurate photothermal therapy at facile temperature. *Nature Communication*, 2016, **7:** 10437–10.

[51] ZHENG M B, YUE C X, MA Y F, *et al*. Single- step assembly of DOX/ICG loaded lipid-polymer nanoparticles for highly effective chemo-photothermal combination therapy. *ACS Nano*, 2013, **7(3):** 2056–2067.

[52] SHUKLA N, SINGH B, KIM H J, *et al*. Combinational chemo-therapy and photothermal therapy using a gold nanorod platform for cancer treatment. *Particle & Particle Systems Characterization*, 2020, **37(8):** 2000099–15.

[53] MENG Z Q, WEI F, WANG R H, *et al*. NIR- laser-switched *in vivo* smart nanocapsules for synergic photothermal and chemotherapy of tumors. *Advanced Materials*, 2016, **28(2):** 245–253.

掺钕介孔硼硅酸盐生物活性玻璃陶瓷骨水泥的制备与性能表征

陈 铖[1], 丁晶鑫[1], 王 会[2], 王德平[1]

(1. 同济大学 材料科学与工程学院, 上海 201804; 2. 上海中医药大学 康复科学学院, 康复医学研究所, 中医药智能康复教育部工程研究中心, 上海 201203)

摘 要: 骨肉瘤是一种常见的恶性骨肿瘤, 常通过手术切除进行治疗。但术后造成的骨缺损难以自愈, 残余肿瘤细胞还会增加复发可能性。本研究开发了一种用于修复骨缺损和协同治疗骨肉瘤的掺钕介孔硼硅酸盐生物活性玻璃陶瓷骨水泥。首先通过溶胶–凝胶法结合固态反应制备了可作为光热剂和药物载体的掺钕介孔硼硅酸盐生物活性玻璃陶瓷微球(MBGC-*x*Nd), 然后将微球与海藻酸钠(SA)溶液混合制备了可同时进行光热治疗和化学治疗的可注射骨水泥(MBGC-*x*Nd/SA)。结果表明掺 Nd^{3+}赋予微球可控的光热性能, 负载阿霉素(DOX)的微球显示出持续的药物释放行为。此外, 载药骨水泥的药物释放量随着温度的升高而显著增加, 说明光热疗法产生的热量可促进 DOX 释放。体外细胞实验结果表明, MBGC-*x*Nd/SA 具有良好的促成骨活性, 并且光热–化学联合疗法对 MG-63 骨肉瘤细胞起到了更显著的杀伤作用, 表现出协同效应。因此，MBGC-*x*Nd/SA 作为一种新颖的多功能骨修复材料, 在骨肉瘤的术后治疗方面具有良好的应用前景。

关 键 词: 掺钕介孔硼硅酸盐生物活性玻璃陶瓷; 骨水泥; 骨缺损修复; 光热–化学联合疗法

中图分类号: R318 **文献标志码:** A